Supplementary Information for

"*In situ* Characterization of Kinetics and Mass Transport of PbSe Nanowire Growth *via* LS and VLS Mechanisms"

Miao Song,[a] Jaewon Lee,[a] Bin Wang, [a, b] Benjamin A. Legg,[a] Shenyang Hu,[c] Jaehun Chun,[a]

Dongsheng Li[*a]*

[a.] *Physical and Computational Sciences Directorate, Pacific Northwest National Laboratory, Richland, WA 99352, USA.*

[b.] *School of Science, MOE Key Laboratory for Non-equilibrium Synthesis and Modulation of Condensed Matter, State Key Laboratory for Mechanical Behavior of Materials, Xi'an Jiaotong University, Xi'an, 710049, China*

[c.] *Energy and Environment Directorate, Pacific Northwest National Laboratory, Richland, WA 99352, USA*

* E-mail: Dongsheng.Li2@pnnl.gov

This file includes:

1. Experimental

The catalyst bismuth powder (Bi, purity ≥99.99%, Sigma-Aldrich) and the precursor material lead selenide (PbSe, purity 99.99%, Sigma-Aldrich) were gridded and dispersed in ethanol at a molar ratio of 1/2. The liquid (particle size < ~1 μm) was then drop-cast onto TEM heating chips of the gas cell (Fig. S1). In our work, two types of experiments were employed including *in situ* HRTEM experiment and in situ low magnification (LM) TEM experiment.

During the *in situ* HRTEM experiment, two types of gas cell heating holder with gas flow and pressure control were used: a Climate sample holder (DENSsolutions, The Netherlands) for HRTEM and an atmosphere holder (Protochips, USA) for EDS. Only limited precursor powders can be drop-casted onto one of two gas heating TEM chips to avoid breaking SiNx membrane. A forming gas of 5 vol% H_2 in N_2 was used for PbSe nanowire growth and the flow rate was 0.2 ml/min. Before heating, the forming gas was flowed into the assembled gas cell in a TEM holder at a pressure of (4~5) $\times 10^3$ Pa for ~5 min. The gas cell was then sealed and TEM chips were heated from room temperature to 900 or 950°C directly at a rate of 10°C/s and held at this temperature for ~5 min to dissolve enough precursor in the Bi liquid catalyst droplet. The temperature was then ramped down to 525°C within 1 min (10°C/s) for PbSe nanowire growth with the gas flow at a pressure of (4~5) $\times 10^3$ Pa (Fig. S2). Due to the limited amount of precursor on the heating chips, no nanowire growth was observed during the *in situ* HRTEM experiment without initial 900°C heating. An aberration-corrected environmental TEM (ETEM), equipped with an OneView camera (Gatan, USA), was employed at 300 kV for imaging. *In situ* HRTEM images were recorded at a rate of 25 frames per second with an electron dose rate of ~10^4 $e \cdot nm^{-2} \cdot s^{-1}$. Another aberration-corrected ETEM, equipped with a high-angle annular dark-field (HAADF) detector and a Super-XTM EDS detector system, was employed at 200 kV for HAADF scanning TEM (STEM) and in situ composition analysis at 525°C. Notably, due to the fast growth process of stage I (~54 s, Fig. 1 and 4), we were not able to acquire *in situ* EDS data during stage I. Pb element in liquid catalyst droplets comes from the decomposition of precursor powders of PbSe.

On the other hand, in the *in situ* LM TEM experiment, A 652 furnace heating holder (Gatan, USA) was used. A large amount of precursor powders was sandwiched by a SiN_x TEM chip and a carbon grid and heated to target temperatures (575°C and 600°C) under the mixed gas conditions (5 vol% H_2 in N_2) at a pressure of 8 $\times 10^2$ Pa.

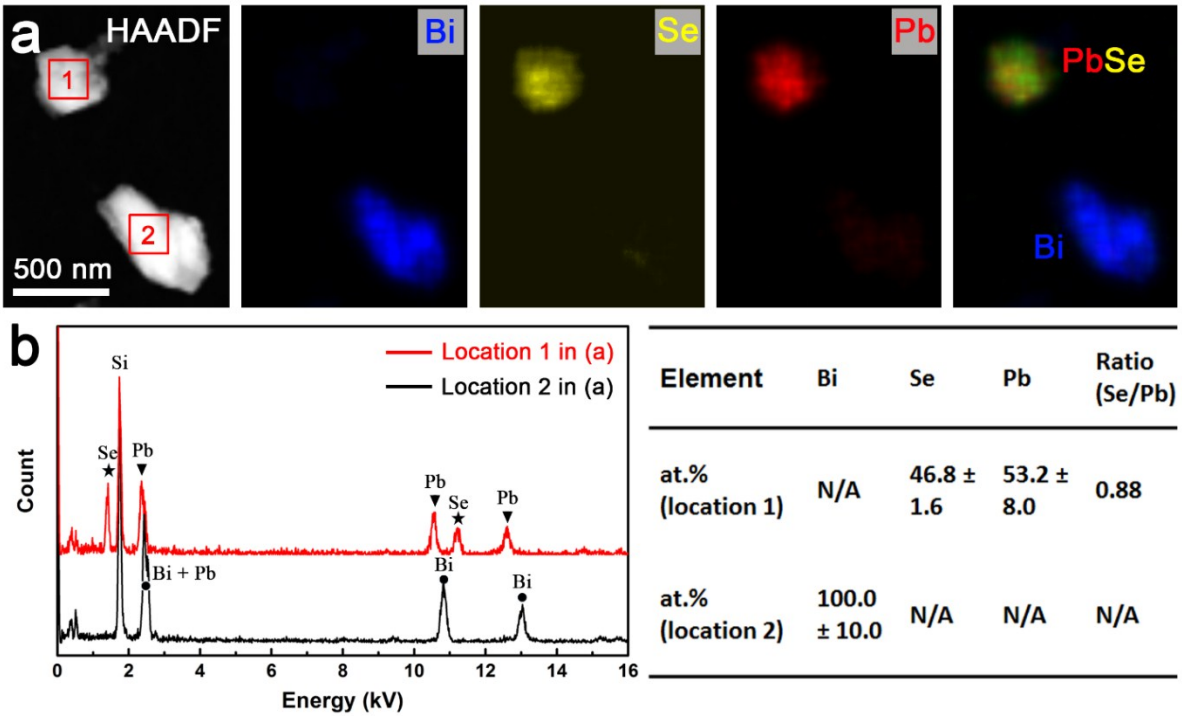

Element	Bi	Se	Pb	Ratio (Se/Pb)
at.% (location 1)	N/A	46.8 ± 1.6	53.2 ± 8.0	0.88
at.% (location 2)	100.0 ± 10.0	N/A	N/A	N/A

Fig. S1 Composition analysis before heating. (a) EDS mapping of Bi and PbSe particles. (b) EDS spectra of the Bi and PbSe particles in (a) and atomic percentage (at. %) of Bi, Se, and Pb. Errors come from the EDS analysis software. The signal of Si was from SiN_x films of heating chips.

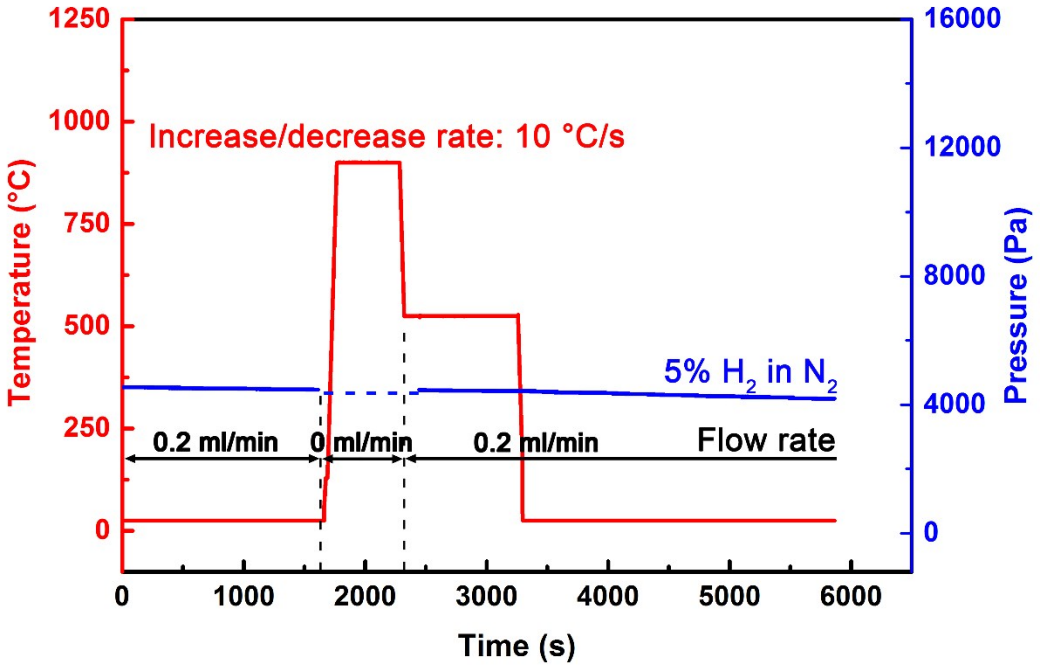

Fig. S2 Profile of temperature and gas during an *in situ* heating experiment.

2. Morphological evolution during *in situ* heating

When TEM chips were heated up to 900°C, the Bi catalyst became amorphous liquid droplets of tens of nanometers size (indicated by white arrows, Fig. S3a), and PbSe volatilized partially with the formation of vapors of the growth species. Reserved PbSe particles (indicated by red arrows in Fig. S3b) can supply a growth precursor of PbSe nanowire continuously during the subsequent VLS growth process after cooling from 900°C to 525°C due to evaporation of PbSe at 525°C. Chips were kept at 525°C with mixed gas (5 vol% H_2 in N_2) flowing at a pressure of (4~5) $\times 10^3$ Pa by using a Protochips Aduro heating holder. As illustrated in Fig. S3c-f, PbSe partially dissolved after 60 min at 525°C, which verified that during the *in situ* heating process reserved PbSe precursor can evaporate continuously to supply growth precursor.

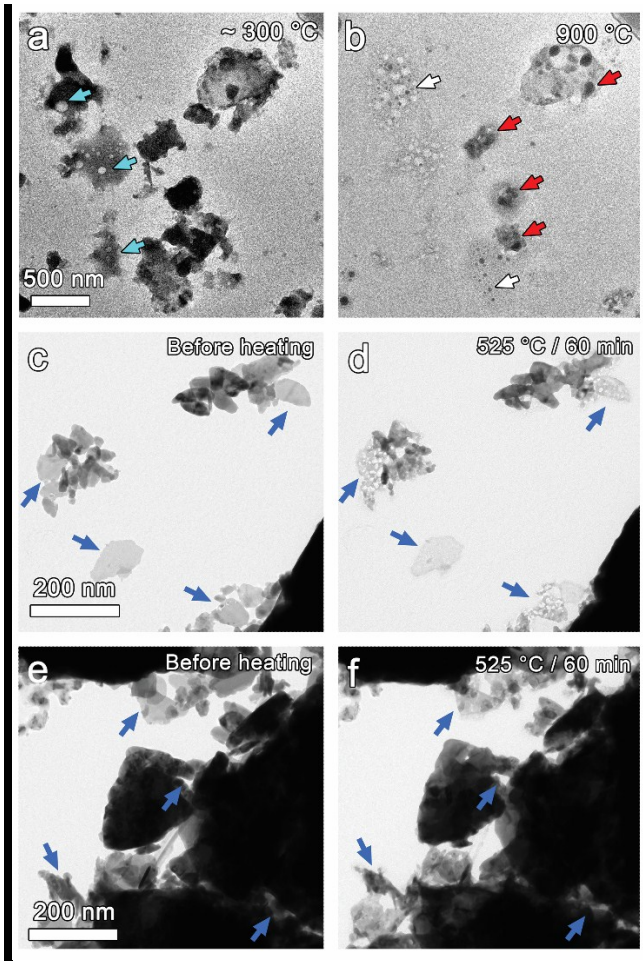

Fig. S3 Phase change of Bi and PbSe particles during heating process. (a) Beginning of Bi liquefaction at ~300°C (indicated by cyan arrows). (b) Formation of liquid droplet promoters (white arrows) when the temperature was increased to 900°C and partial evaporation of PbSe precursor (red arrows). (c-f) Bright field (BF) TEM images showing evaporation of PbSe particles (indicated by blue arrows) at low pressure (8×10^2 Pa) in 5% H_2/N_2 mixed gas at 525°C.

3. The evolution of the curved solid/liquid interface

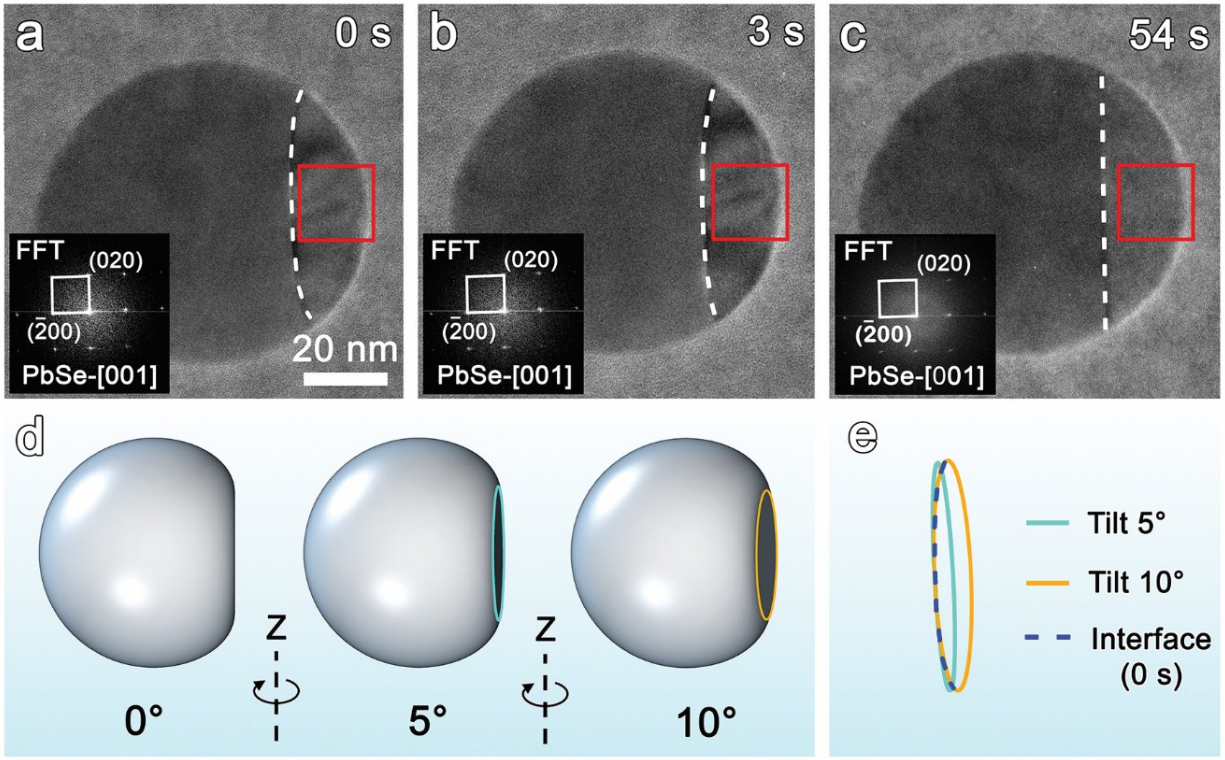

Fig. S4 Evolution of the interface between liquid and PbSe solid. (a-c) HRTEM images of growth stage I. Insets are fast Fourier transform (FFT) images of corresponding red-boxed areas, showing all PbSe present the same zone axis of $[001]$ and (200) planes along the perpendicular direction. (d) Schematic illustration of interface projection under different tilt angles along the Z direction. (e) Outlines of the flat interface projection at different tilt angles and $I_{L/S}$ in (a).

During growth stage I, the solid/liquid interface ($I_{L/S}$) evolved from a curved interface (Fig. S4a) to a straight interface (Fig. S4c). As simulated in Fig. S4d-e, to form the curved interface as shown in the experiment from a flat surface projection, the flat round $I_{L/S}$ needs to be tilted ~10° (Fig. S3e). In addition, when the sphere was tilted, the crystal lattice became striped in the direction perpendicular to the tile axis.[1] However, to acquire an HRTEM image with separated crystal lattice, the largest deviation angle should be less than 2.5° perpendicular to the symmetrical diffraction spots direction (*i.e.*, separated/clear crystal plan) for crystal thicker than 20 nm.[1, 2] Considering the spherical morphology of the whole particle, the thickness around the central interface area in Fig. S3a is ~35 nm. All PbSe crystals were present in the same orientation $[001]$ with symmetrical diffraction spots along $[200]$ direction (see Fig. 1, insets),

proving that the largest tilt angle along the Z axis (Fig. S3d) should be significantly smaller than 2.5°. Therefore, the interface is truly curved and parallel to the electron beam.

4. *Ex situ* EDS analysis after cooling to room temperature

Due to the dramatic change in temperature when cooling from 525°C to room temperature within 1 min, the nanowire in Fig. 1 broke into several parts (Fig. S5a). EDS mappings verified that the original nanowire was composed of Pb and Se, and the droplet was mainly composed of Bi with a small amount of Pb.

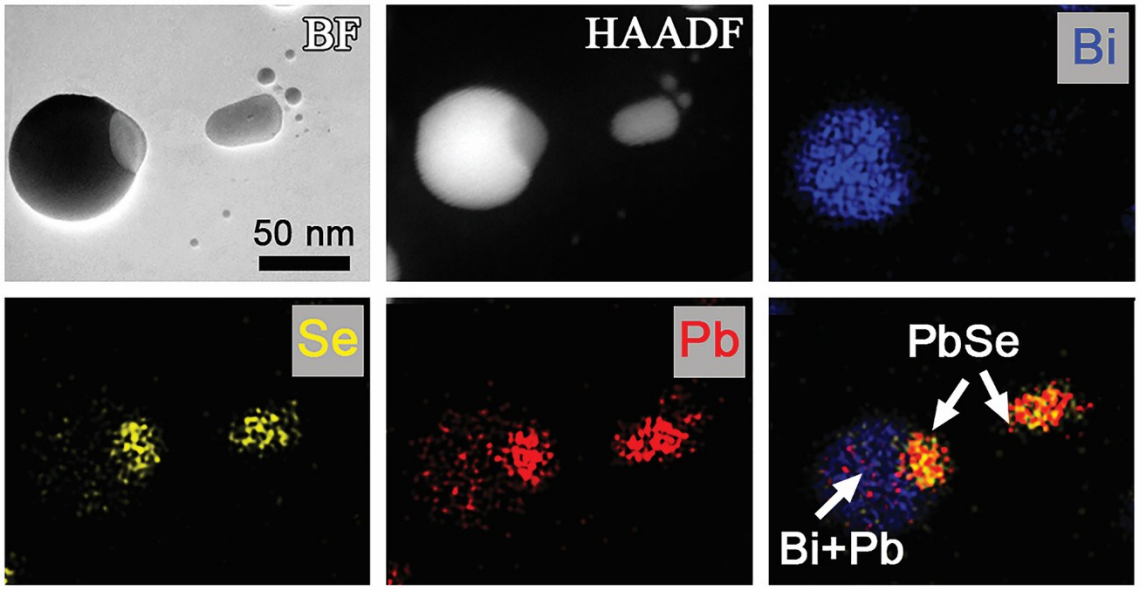

Fig. S5 Composition analysis. (a) EDS mapping of the particle in Fig. 1. BF and HAADF images of the particle after cooling to room temperature and EDS mapping of the broken PbSe nanowire.

5. Surface tension induced lattice strain near the triple-phase interface

The surface tension of vapor-liquid (γ_{VL}), vapor-solid (γ_{VS}), and liquid-solid (γ_{LS}), at the triple-phase interface (Fig. 2c and Fig. S6) induced strain (ε) in PbSe crystal near triple-phase interface (J_{TP}). The γ_{VL} of Bi catalyst liquid (0.35-0.45 J/m^2 [3]) is close to the γ_{VS} of PbSe (0.32-0.42 J/m^2 [4]. γ_{VL} and γ_{LS} cancelled out each other due to ~180° angle between them and the net surface tension at J_{TP} can be considered as γ_{LS}, inducing ε_{XX} and ε_{YY}. Experimental results of ε evolution along the $[200]$ (ε_{XX}) and $[020]$ (ε_{YY}) are consistent with calculation of the x and y components of γ_{LS}.The theoretical spacing of $\{200\}$ of PbSe at 798 K (525 °C) is 3.097 Å (3.061Å at 298 K[5], the linear thermal expansion coefficient of PbSe is $1.46\times10^{-4}K^{-1}$ from 300-900K[6]).

Notably, although the surface tension is associated with composition and temperature, we supposed the surface tension is not changed during initial 11s, because the variation of Pb and Se element in Bi catalyst can be ignored under less volume increasing of PbSe crystal (~ 1.5% of the whole sphere) from 0s to 11s at 525 °C. In addition, due to the obvious evaporation of PbSe crystal during stage II (SI-2), only the evolution of surface tension during stage I was analyzed.

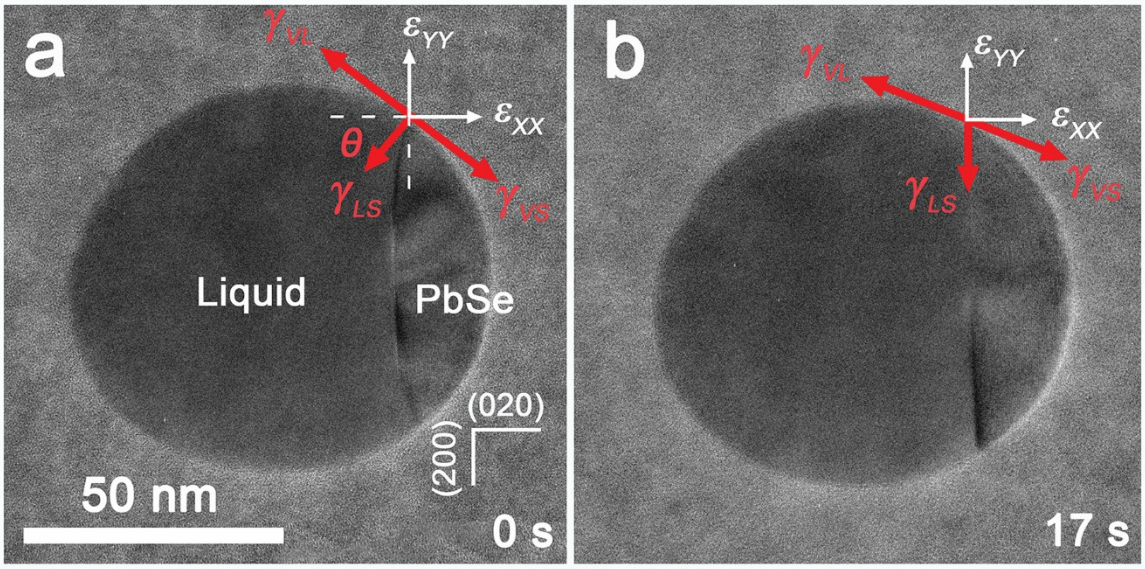

Fig. S6 Relationship of surface tension with $I_{L/S}$. (a) Distribution of surface tension at 0s with a curved $I_{L/S}$. (b) Distribution of surface tension at 11s with a straight $I_{L/S}$.

6. Two nucleations in one droplet

Another nucleus was also detected on the liquid droplet surface of the particle in Fig. 1 (Fig. S7a). However, the nucleus did not grow into a nanowire after a long heating process (Fig. S7c). This small nucleus formed proximately at the same nucleation stage of the right PbSe crystal (stage I) and was also induced by supersaturated growth species in the liquid promoter when decreasing the temperature from 900°C to 525°C. After nucleation, only one nucleus grew into the nanowire. This is associated with the finite volume of the liquid sphere, which cannot supply enough precursors for two-nanowire growth[7]. Notably, most of the particles just have one nucleus in each catalyst droplet (Fig. S7g-i).

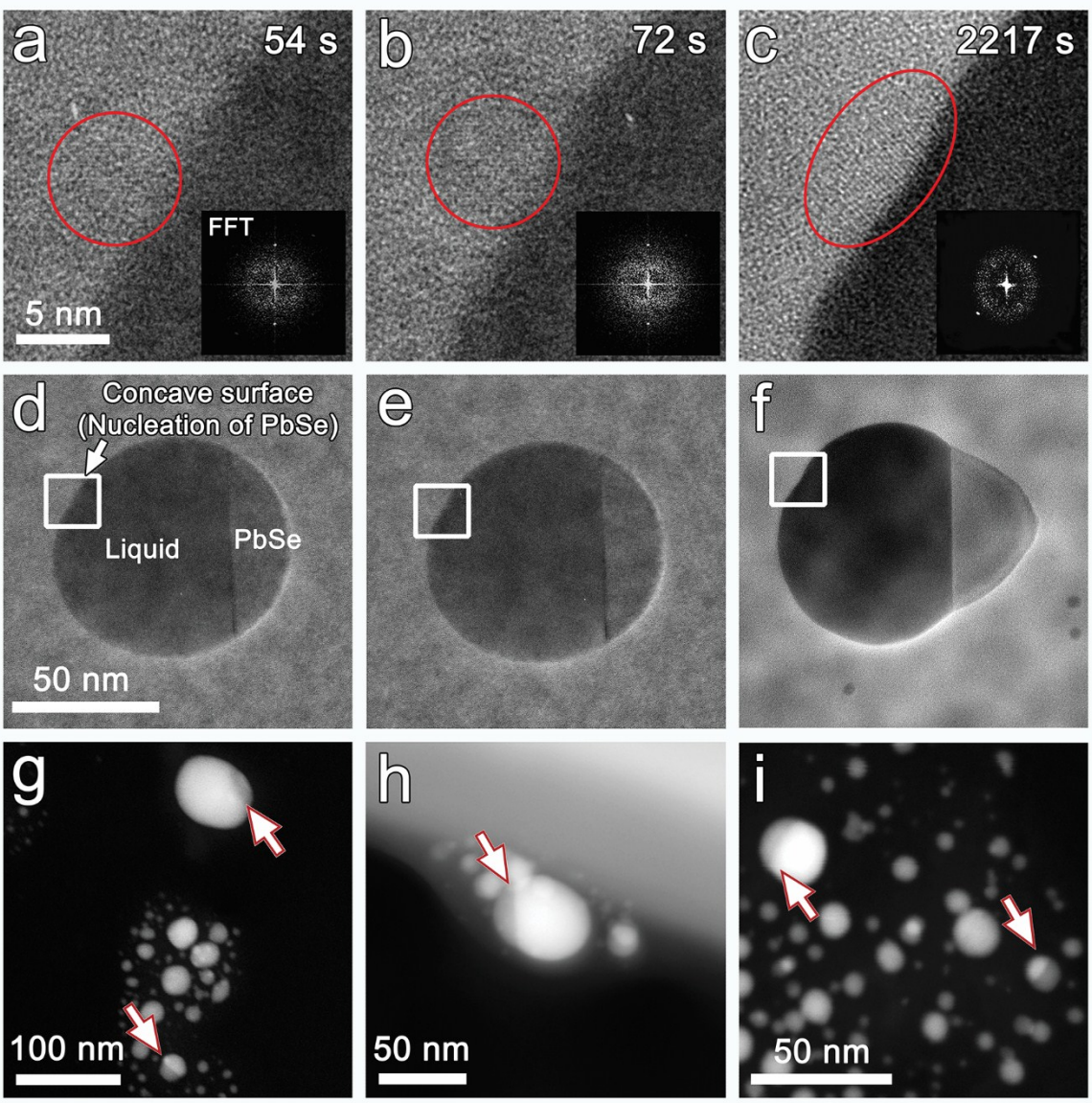

Fig. S7 Two nuclei on one promoter droplet. (a-c) Enlarged images of white-boxed areas in (d-f), respectively, showing another nucleation of PbSe on the Bi liquid sphere at 525°C with formation of concave surface on liquid surface. (g-i) Other examples showing that only one nucleus is formed in each catalyst droplet. Nucleated particles are denoted by white arrows.

7. Supersaturated growth species at stage I

Based on TEM BF images before heating (~8.3 % of the area was covered by particles, average particle thickness ~250 nm, the area of the heated region is 300 × 300 μm^2, and the gas cell spacing is 2 μm), estimated PbSe powder in the heated area is ~3.5 × 10^{-10} mol. Meanwhile, in terms of the weight of precursors dropped on TEM chips, the estimated PbSe is ~5.9 × 10^{-10} mol on the heating area (1.9 × 10^{-7} mol PbSe powder was drop-casted on a circle

chip area with a radius of 3 μm; the mole ratio of Bi/PbSe is ~1/2). Therefore, PbSe is (3.5–5.9) × 10^{-10} mol and almost 2 ~ 4 times of the filled H_2 (~1.5 × 10^{-10} mol, 5 vol. % H_2 in N_2) in the static sealed TEM cell when holding at 900–950°C. This means that even though all the H_2 reacted with Se vapor[8] in the sealed cell, more than ~57% of the PbSe remained in the sealed heated space. The remaining PbSe evaporated and dissolved into liquid promoter spheres and induced nucleation of PbSe crystal at stage I, due to a larger accommodation coefficient of liquid droplets.[9] This is also verified by two nuclei on one promoter droplet (Fig. S7a-f).

In terms of the precipitation process of supersaturated Se precursor from a liquid promoter at stage I, the estimated supersaturated concentration of Se precursors based on a 2D projection image (Fig. 1c) at the beginning of stage I in our experiment is ~18 at. %. Based on a Bi-Se phase diagram,[10] if all reserved PbSe precursor dissolved into the Bi liquid promoter uniformly, the concentration of Se precursor (even excluding possible H_2Se) in Bi promoter should be ~57 at. %, which is higher than the calculated supersaturated concentration at the beginning of stage I (~18 at. %) analyzed above. Therefore, ~18 at. % supersaturated concentration of Se precursor is reasonable.

8. Length measurement standard and growth mechanism during stage II

The exact location of the interface $I_{L/S}$ (the 119th layer) was identified by the lattice intensity profile derived from the HRTEM image of the PbSe crystal (Fig. S8a-b and f-g), wherein, the 1st layer and then119th layer of $\{200\}$ from the right tip of the PbSe crystal are denoted by red lines. The intensity of the 119th layer at the interface central area remained almost unchanged with further heating at 525°C for 24 s (Fig. S8h) compared with that of 2563 s (Fig. S8c). There is a newly formed step (two layers of $\{200\}$ plane) on the 119th layer near the top triple phase boundary (Fig. S8i) at 2587 s in contrast to the previous image at 2563 s (Fig. S8d), but no obvious lattice change was detected at other areas on the $I_{L/S}$, such as the bottom area (Fig. S8e and j). This corresponds to a mono-nucleus layer-by-layer growth mechanism, *i.e.*, a step nucleated on $I_{L/S}$ at the triple phase boundary first, and then the step epitaxially and laterally grows across the area of the previously formed $\{200\}$ plane before the next nucleation inducing the growth of the PbSe wire along the $\langle 100 \rangle$ direction.

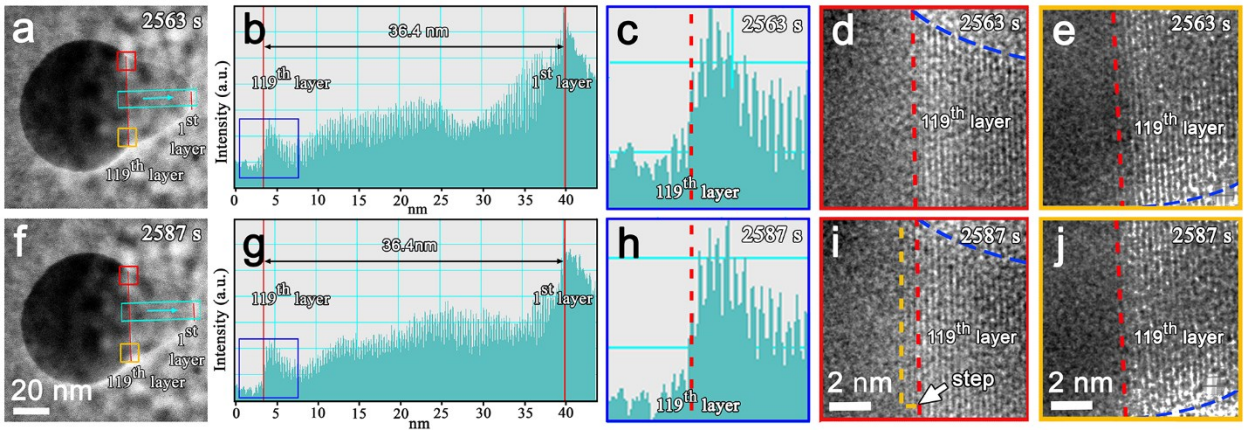

Fig. S8 The growth mechanism of stage II. (a) and (f) HRTEM images of PbSe nanowire during the VLS growth process at 2563 s and 2587 s, respectively. (b) and (g) Intensity profiles of cyan-boxed areas along arrows direction in (a) and (f), respectively, showing the location of the 119th layer. (c) and (h) Enlarged blue-boxed areas in (b) and (g), respectively. (d) and (i) Enlarged red-boxed areas in (a) and (f), respectively. A newly formed step at 2587 s is denoted by yellow dashed lines. (e) and (j) Enlarged yellow-boxed areas in (a) and (f), respectively. The 119th layer is denoted by red dashed lines.

9. Direct observation of PbSe wire growth by VLS mechanism

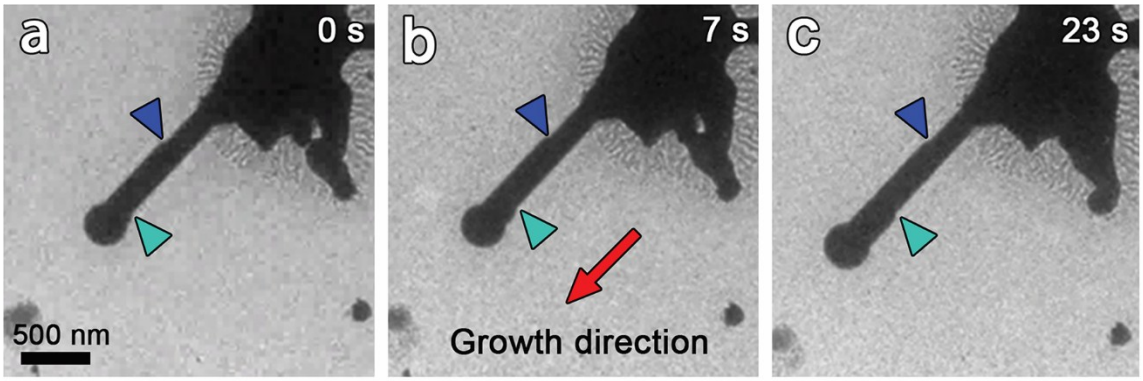

Fig. S9 *In situ* low magnification experiment. Sequence TEM images of PbSe wire growth via VLS at 575°C. Blue and cyan arrows show two steps on the wire, showing the movement of the liquid promoter and the growth of the of PbSe wire.

PbSe wires were obtained by conducting an *in situ* low magnification (LM) heating experiment with a 652 Gatan heating holder in the mixed carrier gas (5 vol% H_2 in N_2) environment under a pressure of 8×10^2 Pa. Fig. S9 presents the growth process of a PbSe wire at 575°C (see also Movie S2). Blue and cyan arrows present the same locations of the PbSe

wire during the growth process, indicating that PbSe grew along the red arrow direction by the VLS mechanism. The calculated growth rate of the PbSe wire in Fig. S7 is ~9.8 nm/s.

10. Step-growth mechanism on top {200} surface

The selected area electron diffraction (SAED) pattern with several degrees of sample tilt (Fig. S10b-c) along the $[001]$ zone axis verified that the elongated direction of the PbSe wire is $\langle 100 \rangle$. The SAED pattern shows that the four side surfaces are {200} planes (Fig. S10d). In the *in situ* LM experiment, we found some steps (Fig. S10d-e and g-i) on (200) surface, which was original liquid/solid interface during growth process. These steps were associated with the unfinished lateral growth process after nucleation of a mono-nuclear step consisting of a growth mechanism at stage II (Fig. 3e-h, and Fig. S8); *i.e.*, after nucleation, the layer grows laterally from one side of (020) to another across the (200) plane (Fig. 3h). The curved growth front of the steps on the growth interface was induced by the diffusion difference between the bulk and near surface in liquid droplet.[11]

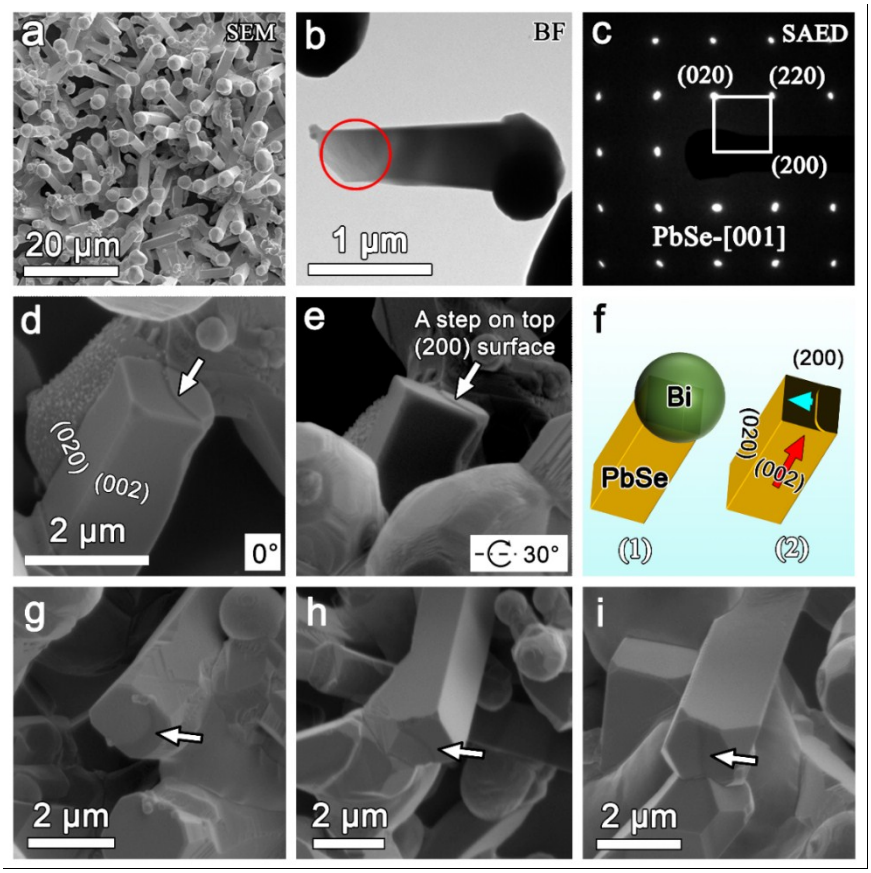

Fig. S10 Steps on $I_{S/L}$ interfaces. (a) SEM image of PbSe wires grown in a Gatan heating holder at 600°C. (b) BF image of a PbSe wire. (c) SAED of the red circle area in (b). (d) and (e) SEM images showing the same step on the top {200} surface (original $I_{S/L}$ interfaces) at different tilt

angles. (f) Schematic illustration of a step on the original liquid/solid interface. (g-i) Other three examples showing steps (denoted by white arrows) on top {200} surfaces.

11. Vapor species in TEM heating cell during heating

During the *in situ* experiment, a carrier gas (5 vol% H_2 in N_2, 0.2 ml/min) at a pressure of (4~5) $\times 10^3$ Pa was flowed into a TEM holder for ~5 min keeping the whole TEM cell spacing filled with the carrier gas. Then the gas cell was sealed and the TEM chips were heated from room temperature to 900–950°C directly and held at 900–950°C for ~5 min to dissolve enough precursor. The temperature was then decreased to 525°C for PbSe nanowire growth with the carrier gas flowing under the same conditions as before heating. Here, we used binary phase diagrams (Fig. S11) and *in (ex) situ* EDS results to analyze vapor phases in the TEM gas cell during the experiment.

Based on the Bi-Pb phase diagram (Fig. S11b), Pb is soluble in Bi liquid at miscible atomic percentages above 327°C. This is consistent with experimental EDS results (Pb, from 0 to 85%, Fig. S6b and Fig. 3c). No Se element was detected in the Bi liquid droplet. PbSe decomposed during the heating process with formation of PbSe and Se vapors, respectively.[12] The vapor pressure (*P*) of PbSe and Se can be calculated based on the following equation:

$$\log P\,[Pa] = A - BT^{-1} \quad (1)$$

where A and B are the coefficients and T is temperature (K). For Se vapor, A is ~6.016 and B is ~11120.4; for PbSe vapor, A is ~7.528 and B is 11433.[13] Therefore, the theoretical equilibrium partial pressure of PbSe and Se at 525°C is ~1.6 × 10^{-7} Pa and ~1.2 × 10^{-8} Pa and at 900°C ~ 6.0 × 10^{-3} Pa and 3.4 × 10^{-4} Pa, respectively.

Se vapor can react with H_2 at 400–685°C to form H_2Se.[8] Therefore, in TEM heating cells, four kinds of vapors are associated with original PbSe precursor: PbSe, Pb, Se, and H_2Se. Based on the Bi-Se binary phase diagram, the equilibrium solubility of Se in Bi is ~ 25 at. % at 525°C, but no Se was detected during the VLS growth process (Fig. 4). In addition, the partial pressure of PbSe and Se at 525°C is ~1.6 × 10^{-7} Pa and ~1.2 × 10^{-8} Pa, and H_2Se gas has a partial pressure of ~200 Pa (5 vol. % H_2 in mixed carrier gas at a pressure of 4×10^3 Pa) assuming Se vapor was enough and reacted fully with H_2 in the sealed TEM cell. Therefore, Se growth species are not supplied from the liquid catalyst droplet during the steady-state VLS growth process.

During stage I, supersaturated growth species (PbSe, Pb, and Se vapors) in the sealed TEM cell dissolved into liquid catalyst droplets, inducing nucleation and growth of PbSe crystal by the LS mechanism. During stage II, due the consumption of Se growth species in the droplet

(no Se detected, Fig. 4), Se was supplied by vapors that reacted with the Pb precursor at the triple phase interface, directly inducing nucleation and growth of the PbSe nanowire during the steady-state VLS growth process. Possible chemical reactions in the TEM cell are as follows:

- During heating at high temperature (900°C–525°C): $PbSe\ (s) \rightarrow Pb(g) + Se(g) + \ PbSe\ (g)$
- In the H_2/N_2 mixed gas: $Se(g) + H_2(g) \rightarrow H_2Se(g)$
- At liquid promotor surface or triple phase boundary: $Pb\ (l) + H_2Se(g) \rightarrow H_2(g) + PbSe(s)$.

Our EDS in Fig. 3c shows no Se in the Bi liquid droplet and is similar to a previously reported *ex situ* experiment.[14] In addition, $PbCl_2$ and S were employed as VLS growth precursors of PbS nanowire, proving the concept that binary nanowires grow with separated pathways of precursor transport.[15]

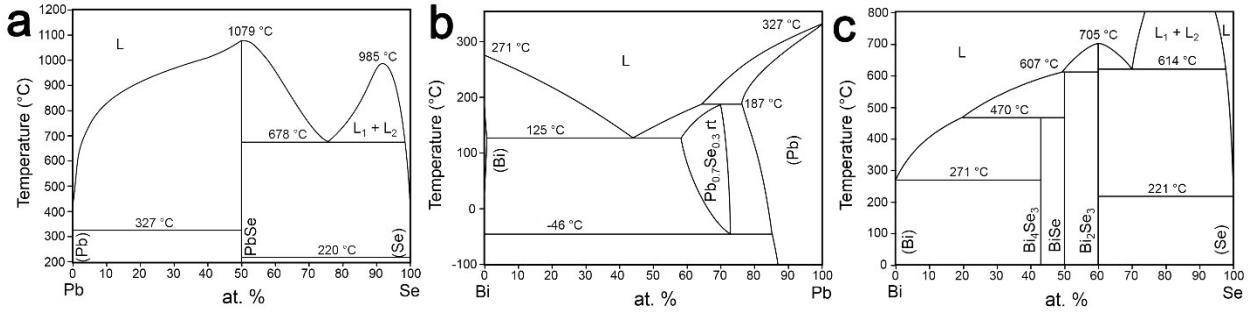

Fig. S11 Binary phase diagrams. (a) Pb-Se[12], (b) Bi-Pb[10], and (c) Bi-Se[10].

12. Nucleation rate and layer growth rate

During the LS growth process, 5 nuclei (islands) were detected on $I_{L/S}$ at 11 s, the nucleation time is ~1–2 s (2 s used for calculation), and the interface radius (r) is ~33 nm (Fig. S12a). Notably, all this was measured based on the 2-dimensional HRTEM image. Therefore, the calculated minimum nucleation rate I_n is $\sim 7.3 \times 10^{-4}$ nm^{-2}·s^{-1}. The lateral growth rate from newly formed nuclei (v) can be estimated by average vertical growth rate (~ 3.3 nm/min) and the nuclei spacing during stage I (13.2 nm, Fig. S12a). The average height of the nucleus is ~6 layers (~1.8 nm, Fig. 3a), the average half nuclei spacing is 33 nm/5 nuclei = 6.6 nm, and the lateral average growth time of these nuclei is ~34 s (6 layers, and 2 s nucleation). Therefore, v is 0.19 nm·s^{-1} and the calculated minimum parameter of $\alpha_{min} = \pi I_n R^3 / v = 434 \gg 1$. When $\alpha \gg 1$, $V = h(\pi v^2 I_n / 3)^{1/3}$. Therefore, the estimated growth rate *V* is ~5.4 nm/min.

During the VLS growth process (stage II), there is one nucleus (two layers of (200) plane) on $I_{L/S}$ at 2587 s and the interface radius is ~28 nm (Fig. 3f-g, Fig. S12b). Generally, the nucleation rate during the VLS growth process is significantly longer than the lateral growth process. For example, the nucleation time for a Si nanowire during the VLS growth process is ~119/120 of

the one layer of growth.[16] In the *in situ* LM heating experiment, ~1/23 of the wire top surfaces have steps indicating nucleation took longer time than the layer lateral growth. The nucleation and the layer lateral growth time are considered to be same: 50 s, *i.e.*, 1/2 of two layers of vertical growth (growth rate is ~0.36 nm/min, Fig. 3f and Fig. 5) corresponding to a maximum I_n and a minimum v. Therefore, I_n is 8.1×10^{-6} nm^{-2}·s^{-1}, v is 0.92 nm·s^{-1} and the calculated maximum parameter $\alpha_{max} = 0.6 < 1$. Generally, the nucleation time is significantly longer than that of the lateral growth during VLS growth process, corresponding to a much larger v than that used in the calculation, and leading to a much smaller real α. When $\alpha \ll 1$, $V = h\pi R^2 I_n$. Therefore, the estimated V of stage II is ~0.72 nm/min.

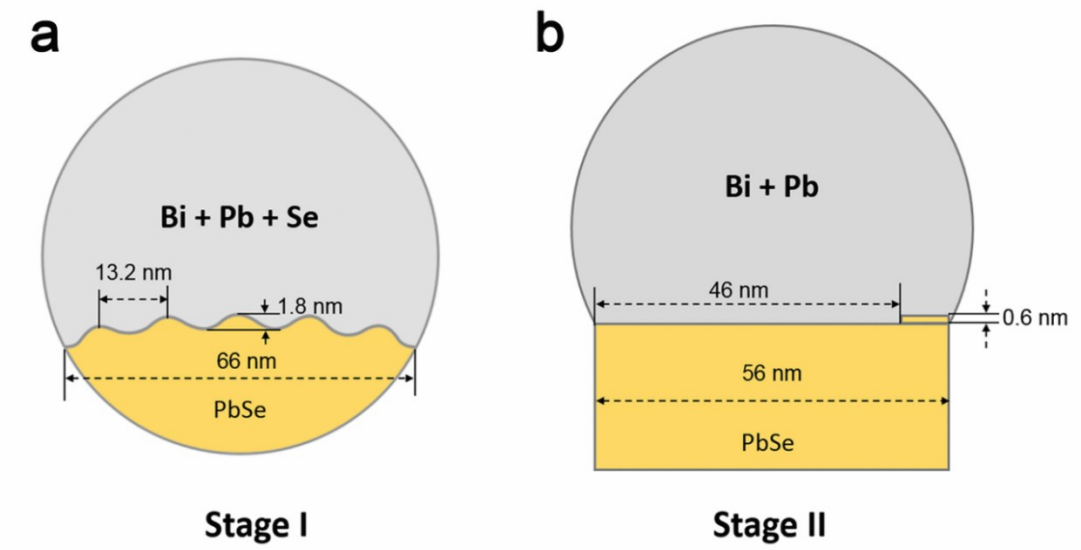

Fig. S12 Schematic illustrations of the two-dimensional spacing of nuclei on $I_{L/S}$ during stage I (a) and the step size during stage II (b) based on *in situ* HRTEM results in Fig. 2.

13. Growth kinetics based on different growth models

As analyzed above (2), PbSe can evaporate at 525°C at low pressure (~8×10^2 Pa in Fig. S2c-f, ~4×10^4 Pa in the *in situ* HRTEM experiment). In addition, there is a small particle on the nanowire tip during the whole stage II growth process (Fig. S13), indicating no atom migration from wire surface to nanowire tip. Therefore, during PbSe nanowire growth along the $[100]$ direction via the VLS mechanism, PbSe also volatilized, thereby partially reducing the width of the PbSe nanowire (Manuscript Fig. 1i). During the VLS growth process, undissolved PbSe particles after heating at 900–950°C (Fig. S3a-b) can continuously supply precursors for PbSe nanowire growth during subsequent heating at 525°C remaining a steady-state nanowire growth

rate. No significant volume decrease was observed due to evaporation of the Bi liquid droplet (Fig. 1i). The width of PbSe nanowire (Fig. 4**)** is the same as the diameter of the interface due to the short time (less than 10 min) of VLS growth process in TEM.

Notably, the VLS growth rate in the *in situ* HRTEM experiment, ~0.36 nm/min (Fig. 5b), is significantly lower than that of 588 nm/min (9.8 nm/s) in *in situ* LM experiment using a Gatan furnace holder (Fig. S9). This is because the DENSsolutions holder used for the *in situ* HRTEM experiment had a smaller capacity for containing the growth species than the Gatan furnace heating holder used for the *in situ* LM experiments. Correspondingly, the growth step is ~0.6 nm (2 layers of (200) plane, Fig. 3f) significantly smaller than that in *in situ* LM experiment (51±14 nm).

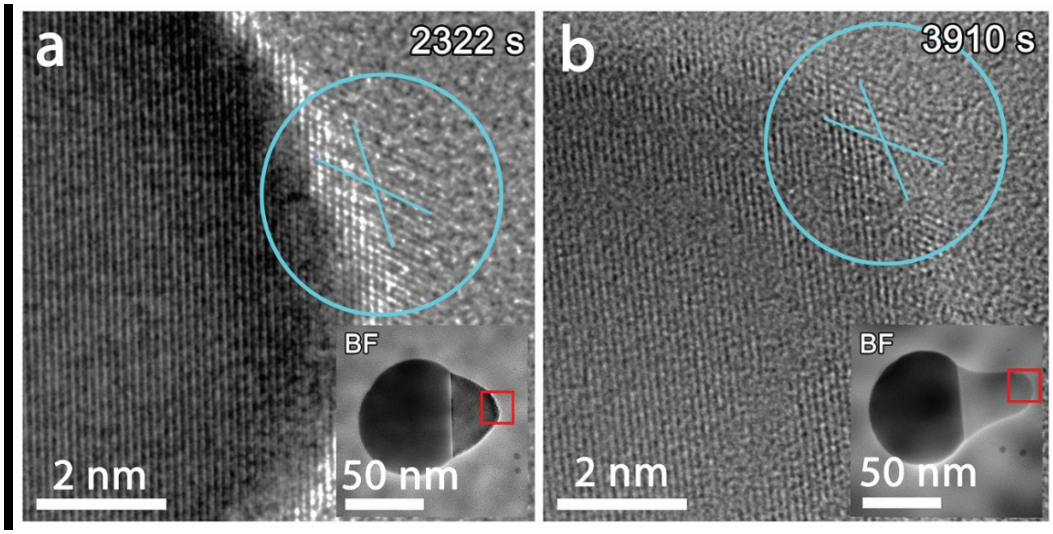

Fig. S13 A small particle on the growing PbSe nanowire tip surface. (a) and (b) HRTEM images of red-boxed areas in corresponding BF images in insets, respectively. Cyan lines denote two lattice directions in the small particle.

14. Width difference in two types of experiments

During the *in situ* HRTEM experiment, a gas heating holder was used and only limited precursor powders can be drop-casted onto one of two gas heating TEM chips to avoid breaking SiN_x membrane. Due to the limited amount of precursor, the width of the rod is approximately tens of nanometers (Fig. 1 and S7). In addition, the wire became thinner (Fig. 1) while growing along [001] direction due to the evaporation of solid PbSe into vapor phase. This evaporation, caused by low concentration of precursor, has been evidenced by heating solid PbSe powers under the similar conditions (Fig. S3c-f).

On the other hand, in the *in situ* LM TEM experiment, a furnace heating holder was used

and a relatively large amount of catalysis and precursor powders was sandwiched between a SiN_x TEM chip and a carbon grid. Long thick PbSe wires (Fig. S14a) grew with a wide size distribution (nanometers to microns, Fig. S10 and Fig. S14) and a high growth rate of 588 nm/min (9.8 nm/s, Fig. S9) in contrast to ~0.36 nm/min in the *in situ* HRTEM experiment (Fig. 5b). In addition, it is obvious that PbSe wires grown on PbSe precursor powders are significantly wider than those grown on TEM grid membrane (Fig. S14a). For both cases, Bi catalyst droplets are needed for wire growth. However, the Bi droplets on the PbSe precursor are bigger than the ones on TEM grid due to the easy liquidation on PbSe precursor powders (Fig. S14b). In addition, a higher concentration of growth precursor gases was supplied near the Bi droplets on PbSe powders by the continuous decomposition of the PbSe precursor powders than near the Bi droplets on TEM grid. Therefore, the wires grew on PbSe precursor powders horizontally and vertically simultaneously and thus thicker than the ones that grew on TEM grid. Therefore, the inconsistency of the width of wires is due to the amount of precursors in the heating cells.

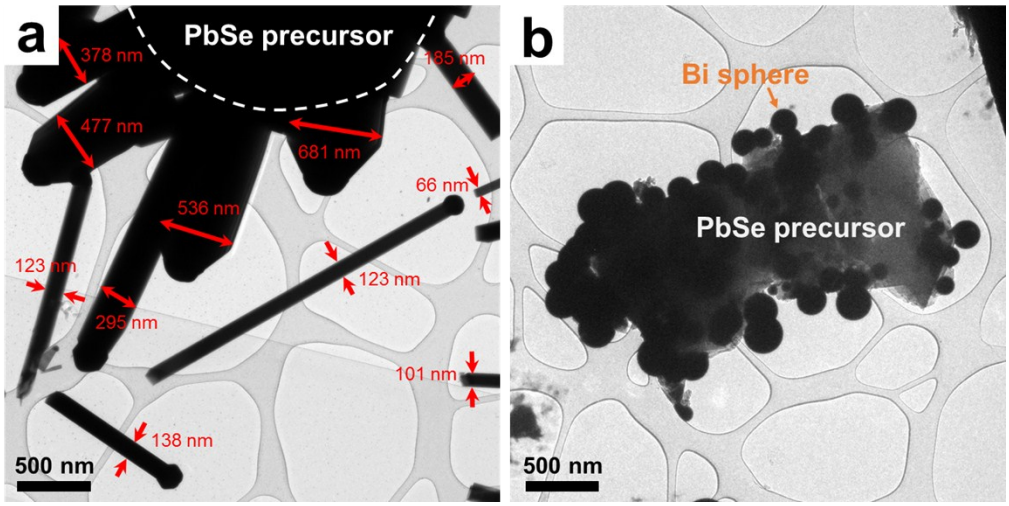

Fig. S14 A large width distribution of VLS grown PbSe wires in the *in situ* LM TEM experiment. (a) Width difference of PbSe wires grown under the same *in situ* LM TEM experiment. (b) Nucleation of numerous of Bi catalyst spheres on PbSe precursor powder at 600 °C.

Reference:

1. Zou, X. D.; Ferrow, E. A.; Hovmöller, S. *Phys. Chem. Miner.* **1995,** 22, (8), 517-523.
2. Hovmöller, S.; Xiaodong, Z. *Microsc. Res. Tech.* **1999,** 46, 147-159.
3. Novakovic, R.; Ricci, E.; Giuranno, D.; Gnecco, F. *Surface Science* **2002,** 515, (2), 377-389.
4. Fang, C.; van Huis, M. A.; Vanmaekelbergh, D.; Zandbergen, H. W. *ACS Nano* **2010,** 4, (1), 211-218.

5. Noda, Y.; Masumoto, K.; Ohba, S.; Saito, Y.; Toriumi, K.; Iwata, Y.; Shibuya, I. *Acta Crystallographica Section C* **1987,** 43, (8), 1443-1445.

6. Sternberg, Y.; Yellin, N.; Cohen, S.; Dor, L. B. *J. Solid State Chem.* **1982,** 43, (3), 364-367.

7. Wu, Y.; Yang, P. *J. Am. Chem. Soc.* **2001,** 123, (13), 3165-3166.

8. Langner, B. E. *Ullmann's Encyclopedia of Industrial Chemistry* **2005,** 32, 343-355.

9. Zhou, G.; Yang, J. C.; Xu, F.; Barnard, J. A.; Zhang, Z. *MRS Proceedings* **2011,** 737, F6.3.

10. Massalski, T. B.; Okamoto, H.; Subramanian, P. R., *Binary alloy phase diagrams*. 2, illustrated, reprint ed.; ASM International: 1990; Vol. 1, p 3542.

11. Wang, H.; Zepeda-Ruiz, L. A.; Gilmer, G. H.; Upmanyu, M. *Nat Commun* **2013,** 4, 1956.

12. Volodin, V. N.; Burabaeva, N. M.; Trebukhov, S. A. *Russ. J. Phys. Chem. A* **2016,** 90, (3), 572-574.

13. Lin, J. C.; Sharma, R. C.; Chang, Y. A. *J. Phase Equilib.* **1996,** 17, 253-260.

14. Bierman, M. J.; Lau, Y. K. A.; Jin, S. *Nano Lett.* **2007,** 7, (9), 2907-2912.

15. Bierman, M. J.; Lau, Y. K. A.; Kvit, A. V.; Schmitt, A. L.; Jin, S. *Science* **2008,** 320, (5879), 1060-1063.

16. Wen, C. Y.; Reuter, M. C.; Bruley, J.; Tersoff, J.; Kodambaka, S.; Stach, E. A.; Ross, F. M. *Science* **2009,** 326, 1247-1250.